LETTER

https://doi.org/10.1038/s41586-018-0707-9

Flight of an aeroplane with solid-state propulsion

Haofeng Xu[1], Yiou He[2], Kieran L. Strobel[1], Christopher K. Gilmore[1], Sean P. Kelley[1], Cooper C. Hennick[1], Thomas Sebastian[3], Mark R. Woolston[3], David J. Perreault[2] & Steven R. H. Barrett[1]*

Since the first aeroplane flight more than 100 years ago, aeroplanes have been propelled using moving surfaces such as propellers and turbines. Most have been powered by fossil-fuel combustion. Electroaerodynamics, in which electrical forces accelerate ions in a fluid[1,2], has been proposed as an alternative method of propelling aeroplanes—without moving parts, nearly silently and without combustion emissions[3–6]. However, no aeroplane with such a solid-state propulsion system has yet flown. Here we demonstrate that a solid-state propulsion system can sustain powered flight, by designing and flying an electroaerodynamically propelled heavier-than-air aeroplane. We flew a fixed-wing aeroplane with a five-metre wingspan ten times and showed that it achieved steady-level flight. All batteries and power systems, including a specifically developed ultralight high-voltage (40-kilovolt) power converter, were carried on-board. We show that conventionally accepted limitations in thrust-to-power ratio and thrust density[4,6,7], which were previously thought to make electroaerodynamics unfeasible as a method of aeroplane propulsion, are surmountable. We provide a proof of concept for electroaerodynamic aeroplane propulsion, opening up possibilities for aircraft and aerodynamic devices that are quieter, mechanically simpler and do not emit combustion emissions.

Electroaerodynamics (EAD) is a means of generating propulsive forces in fluids[1,2]. Ions generated in the ambient fluid and under the influence of an applied electric field are accelerated by the Coulomb force. These ions collide with neutral molecules and couple the momentum of the accelerated ions with that of the bulk fluid; the result is an ionic wind that produces a thrust force in the opposite direction to ion flow. In our device, we generate ions using a corona discharge. A corona discharge is a self-sustaining atmospheric discharge that is induced by the application of a constant high electric potential across two asymmetric electrodes; high electric fields near the smaller electrode accelerate electrons and produce a cascade of ionization by successive electron collisions with neutral molecules[8].

Electroaerodynamic propulsion is a method of manipulating and moving fluids without any need for moving surfaces, making it attractive for a number of applications. For example, the concepts of electrohydrodynamics (where the neutral fluid is water) and electroaerodynamics (where the neutral fluid is air) have been investigated for heat-transfer enhancement[9,10] and ion drag pumps[2].

The additional advantages of being nearly silent and producing no combustion emissions make EAD particularly attractive as a propulsion system for aeroplanes. It could potentially mitigate the harmful impact of current aeroplane propulsion systems on the environment, particularly given the anticipated growth of urban drone usage and its associated noise impacts; EAD could enable the design of quieter, smaller aircraft that interact more closely and innocuously with the urban environment. Its solid-state nature could also enable miniaturization to an extent not possible with conventional propulsion[11]. However, the feasibility of EAD as a method of propulsion is confronted by the challenges of producing sufficient thrust, while achieving low aircraft drag and weight.

Although there have been a number of design proposals for heavier-than-air EAD[6,7] aeroplanes, no such aircraft has yet flown. No other kind of aeroplane with a solid-state propulsion system has flown either (unless supersonic ramjets were to be considered in this category, although the intakes have moving surfaces). This Letter describes the powered flight of such an aeroplane.

A viable propulsion system must produce sufficient thrust without a large weight or drag penalty. This sets limits both on the power requirements (that is, the thrust-to-power ratio) and on the frontal area (that is, thrust density) of the EAD system.

The first of these potential limitations, the thrust-to-power ratio, can be estimated using a one-dimensional steady-state parallel-plate model first presented by Chattock[1] and later experimentally confirmed by Stuetzer[2], and Christensen and Moller[3]. It consists of two electrodes, across which there is a sufficiently high electric potential, resulting in the formation of a small ionization region near the anode and a dominant unipolar conduction region of positively charged ion drift from anode to cathode. The electrostatic behaviour is governed by Gauss's law:

$$\frac{\mathrm{d}E}{\mathrm{d}x} = -\frac{\mathrm{d}^2V}{\mathrm{d}x^2} = \frac{\rho}{\varepsilon_0}$$

where E is the electric field strength, V is the electric potential, ρ is the charge density, ε_0 is the permittivity of free space, and x is the distance along the coordinate direction. Under an inviscid fluid assumption, the fluid momentum equation is governed by the Euler equation: $\mathrm{d}p/\mathrm{d}x = \rho E$, where p is the pressure. The current density $j = \rho(\mu E + v_0)$, where μ is the ion mobility, is composed of the EAD current due to the applied electric field and the convective drift due to the freestream velocity v_0.

Substituting and integrating the above equations gives an analytical equation for the thrust-to-power ratio, which is a measure of static thrust efficiency and an important figure of merit for propulsion systems:

$$\frac{T}{P} = \frac{(\rho\bar{E})LA}{V(jA)} = \frac{\rho\bar{E}L}{V\rho(\mu\bar{E}+v_0)} = \frac{1}{(\mu\bar{E}+v_0)}$$

where T is thrust, P is power, $\bar{E}$ is the average electric field strength, A is the thruster area, and L is the inter-electrode distance. A low average electric field strength $\bar{E}$ gives a higher thrust-to-power ratio, but too low an electric field strength results in no corona inception. Thus there is a limit to the achievable thrust-to-power ratio using the corona discharge. Masuyama and Barrett[5] found experimentally that a thrust-to-power ratio as high as 50 N kW^{-1} was achievable at the laboratory scale, comparable to that of conventional propulsion, where typical performance is about 3 N kW^{-1} for jet engines[12] and about 50 N kW^{-1} for helicopter rotors[13].

A parametric study by Gilmore and Barrett[7] quantified the thrust density of EAD propulsors under a number of different parallel and staged electrode configurations. A trade-off between thrust-to-power ratio and thrust density was identified. At a fixed operating voltage and geometry, an increase in the thrust-to-power ratio results in a decrease in thrust density, and vice versa. The experiments suggested that a thrust density of 3 N m^{-2} and a thrust-to-power ratio of 6.25 N kW^{-1} could be simultaneously achieved with a two-staged configuration of four sets of parallel electrodes. The same configuration is used here (Extended Data Fig. 1).

This level of performance suggested that steady-level flight of a fixed wing unmanned aircraft might be feasible, but at the limit of what is

[1]Department of Aeronautics and Astronautics, Massachusetts Institute of Technology, Cambridge, MA, USA. [2]Department of Electrical Engineering and Computer Science, Massachusetts Institute of Technology, Cambridge, MA, USA. [3]Massachusetts Institute of Technology Lincoln Laboratory, Cambridge, MA, USA. *e-mail: sbarrett@mit.edu

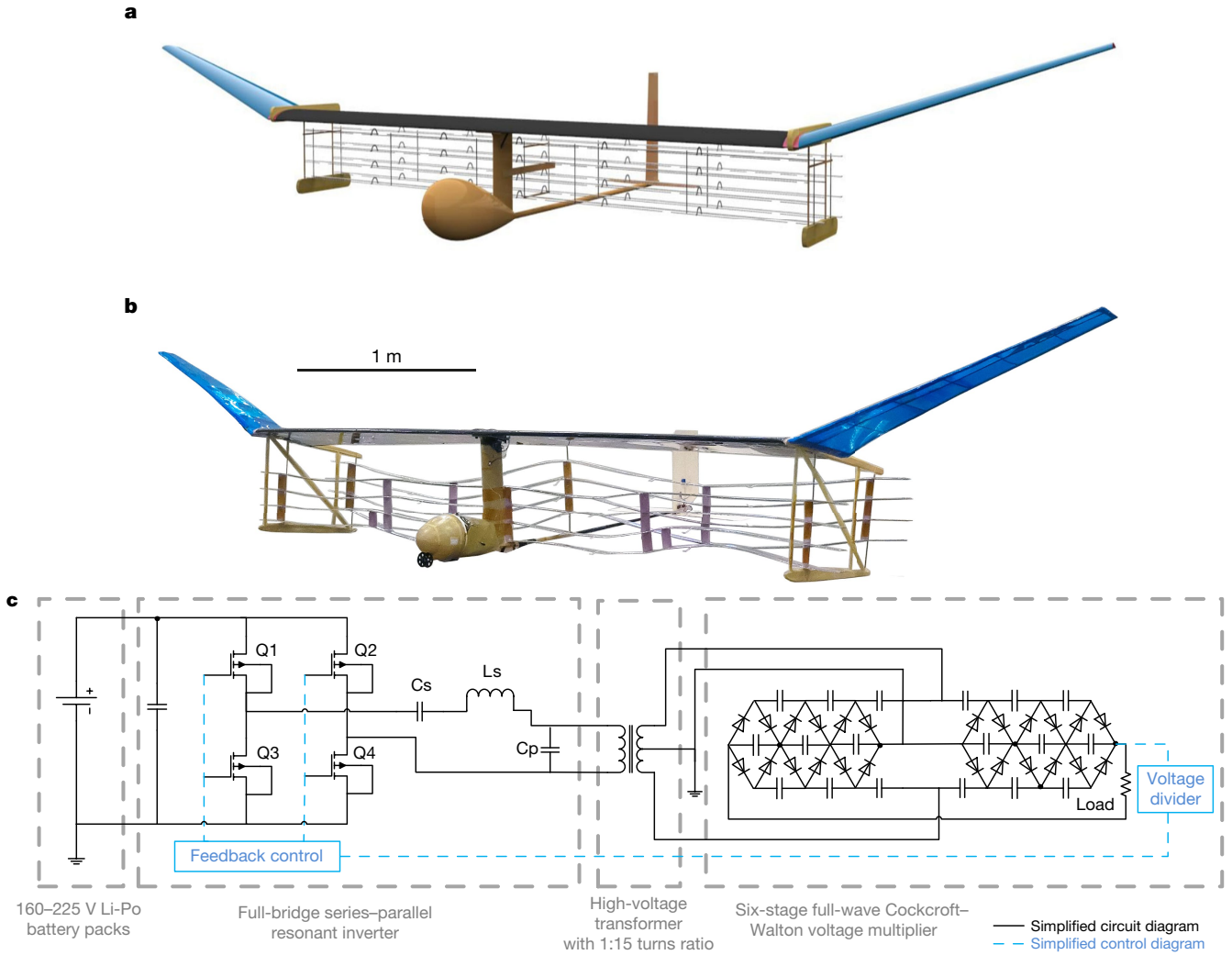

Fig. 1 | Aeroplane design. a, Computer-generated rendering of the EAD aeroplane. **b**, Photograph of actual EAD aeroplane (after multiple flight trials). **c**, Architecture of the high-voltage power converter (HVPC). The HVPC consists of three stages: a series–parallel resonant inverter that converts 160–225 V direct current to a high-frequency alternating current, a high-voltage transformer that steps up the alternating-current voltage, and a full-wave Cockcroft–Walton multiplier that rectifies the high-frequency alternating current back to direct current. The resonant converter uses transformer parasitics (including transformer capacitance) as part of the resonant tank. The three stages contribute a voltage gain of about 2.5×, 15× and 5.6×.

technologically possible using current materials and power electronics technology. It was therefore necessary to systematically search the possible design space for a feasible aircraft design—if one were to exist. We used a geometric programming optimization method to find the most viable size and power for the prototype aircraft design, finding that steady-level flight was just achievable. Geometric programming has been applied to design optimization of conventional aircraft systems[14]. It is able to efficiently find the global optimum of a set of design variables for a certain objective function, given a series of inequality constraints. We chose aircraft wingspan as the objective function to be

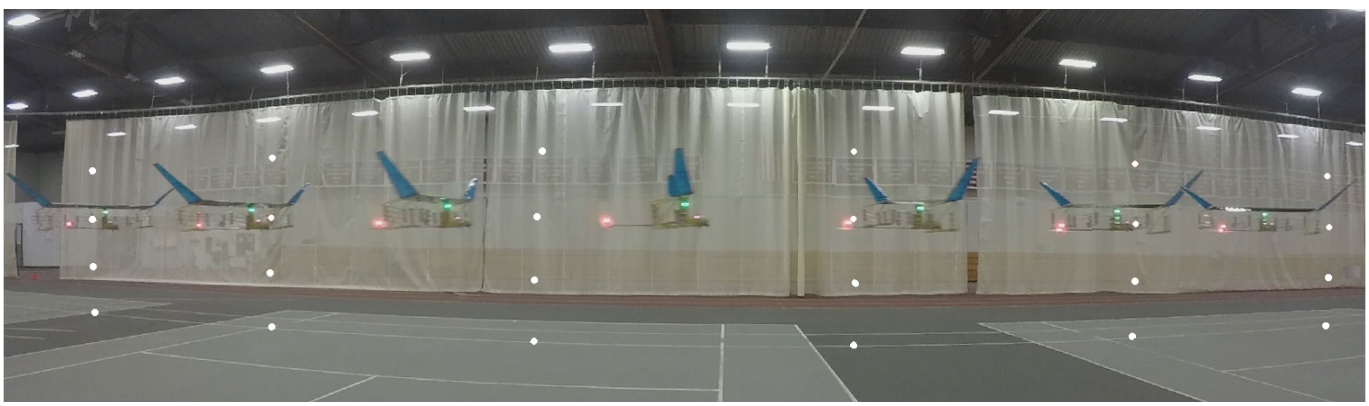

Fig. 2 | Time-lapse image of the EAD aeroplane in flight. White reference markers (spots) are spaced 5 m apart horizontally and 1 m apart vertically. All subsequent results are presented in a Cartesian coordinate system with the *x* axis in the flight direction, *z* axis upwards, and *y* axis pointing away from the camera.

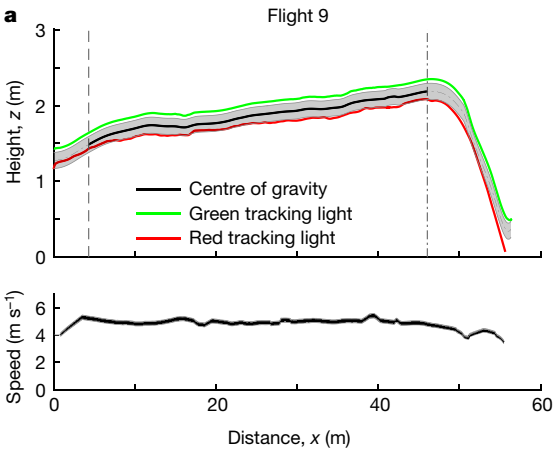

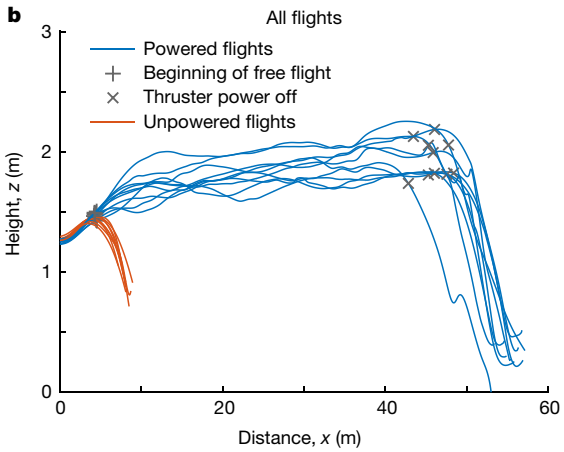

Fig. 3 | Flight trajectories. a, Flight trajectory (top) and speed profile (bottom) for a single flight (number 9): the position of the centre of gravity between launch (vertical dashed line) and propulsion system power-off (vertical dash-dotted line) is shown by the solid black line. The estimated position tracking error is shown in grey (see Methods). **b**, Trajectories for all ten powered flights (blue) and ten unpowered glides (orange). The steady segment of flight covered a distance of 40–45 m with a duration of 8–9 s.

minimized, which corresponds with low weight, low electrical power supply requirements, and low development time, risk and cost. The geometric programming design optimization model incorporated aerodynamic, structural, EAD and power electronics models.

The design optimization was able to find a feasible solution at a wingspan of 5 m with a design weight of 2.45 kg, flight velocity of 4.8 m s^{-1}, thrust of 3.2 N, and electrical power requirement of 600 W (Fig. 1, Extended Data Table 1). We used a conventional tail with elevator and rudder for stability and trim. However, future EAD aircraft without moveable control surfaces are possible.

To produce a sustained thrust of 3 N at the 40 kV design point and estimated thrust-to-power ratio of 6.25 N kW^{-1}, a power system capable of delivering 500 W of output power was required, but at a very low weight. These weight constraints necessitated the design and construction of both a custom battery stack and a custom high-voltage power converter (HVPC) which stepped up the battery voltage to 40 kV. Our HVPC achieved a specific power of 1.2 kW kg^{-1}, 5–10 times higher than conventional power supplies at this voltage and power[15]. This was enabled by careful converter topology selection (Fig. 1c), by design optimization and by operating at a high switching frequency between 500 kHz and 700 kHz to minimize the weight of the capacitors and the magnetics[16,17].

We performed ten flights with the full-scale experimental aircraft at the MIT Johnson Indoor Track (Fig. 2). Owing to the limited length of the indoor space (60 m), we used a bungeed launch system to accelerate the aircraft from stationary to a steady flight velocity of 5 m s^{-1} within 5 m, and performed free flight in the remaining 55 m of flight space. We also performed ten unpowered glides with the thrusters turned off, in which the aeroplane flew for less than 10 m. We used cameras and a computer vision algorithm to track the aircraft position and determine the flight trajectory.

All flights gained height over the 8–9 s segment of steady flight, which covered a distance of 40–45 m (Fig. 3). The average physical height gain of all flights was 0.47 m (Fig. 4a). However, for some of the flights, the aircraft velocity decreased during the flight. An adjustment for this loss of kinetic energy (Fig. 4b) results in an energy equivalent height gain, which is the height gain that would have been achieved had the velocity remained constant. This was positive for seven of the ten flights, showing that better than steady-level flight had been achieved in those cases.

We have thus shown that the feasibility of EAD as a method of propulsion is not prohibited by previously identified limitations in thrust-to-power ratio and thrust density. In this proof of concept for this method of propulsion, the realized thrust-to-power ratio was 5 N kW^{-1}, which is of the order of conventional aeroplane propulsion methods such as the jet engine. However, the overall efficiency was lower than typically achieved by conventional propulsion (and was not the objective here given the limited indoor test area for an uncertified aeroplane). Using the in-flight HVPC power-draw measurements, and confirmation using dynamic wind tunnel experiments, we estimate that the thruster produced 3.2 N of thrust, giving an estimate of overall efficiency:

$$\eta_{\text{overall}} = \frac{T|\vec{v}|}{P_{\text{input}}} = \frac{3.2\,\text{N} \times 4.8\,\text{m s}^{-1}}{600\,\text{W}} = 2.56\%$$

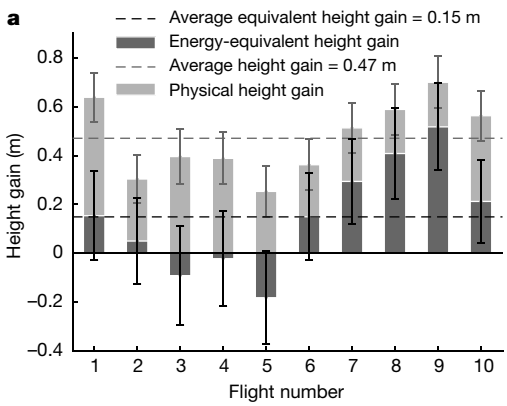

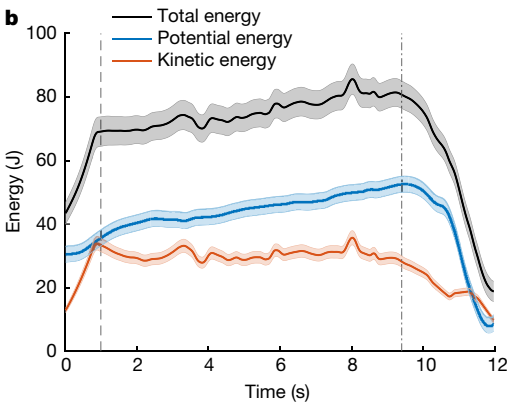

Fig. 4 | Steady-level flight. a, The physical height gain was positive for all flights and the energy-equivalent height gain, which adjusts for the loss of kinetic energy during the flight, was positive for seven flights. Zero energy-equivalent height gain indicates steady-level flight. **b**, The variation in kinetic energy, potential energy and total energy (the sum of kinetic and potential energies) during a particular flight: the potential energy increases substantially, while the kinetic energy remains approximately constant or decreases slightly. Vertical dashed and dash-dotted lines as in Fig. 3a. See Methods for details of error estimation.

which is defined as the thrust power delivered to the aircraft divided by the input electrical power P_{input}; T is the magnitude of the thrust force and $\bar{v}$ is the average velocity of the aircraft in the direction of thrust. To achieve longer range and endurance for practical applications, future research should aim for increasing overall efficiency.

This prototype aircraft was designed by optimizing for small wingspan and low power requirement, which resulted in low overall efficiency, largely due to a low flight speed. This explains the discrepancy between the apparently comparable thrust-to-power performance and the poor overall efficiency performance (which is also a function of the airframe and flight conditions). Using the same EAD performance models and the same aircraft design models, but optimizing for maximum efficiency instead of minimum wingspan, suggests that aircraft with 5% overall efficiency are readily achievable with current technology. This aircraft would be larger, fly faster and require a more powerful HVPC. This design may be useful for applications where low noise and no moving parts are critical, but it is not yet competitive against conventional aeroplanes at similar scale in metrics such as range, endurance and payload capacity.

Further technology improvements in EAD propulsion are needed to increase overall efficiency. Areas include exploring alternative ionization regimes (which could increase practically achievable thrust density and reduce viscous drag from EAD electrodes), designing ways to increase HVPC specific power and efficiency, and integrating the propulsion system with the airframe to reduce the overall aerodynamic power requirements for flight. In the limiting case, one-dimensional EAD theory suggests that overall efficiency for an idealized thruster could be as high as 50%. This would require that a high thrust-to-power ratio be coupled with a configuration that enables higher flight speeds without incurring overwhelming viscous drag[3,5].

Another remaining performance challenge is the achievable thrust density using EAD. Although we have shown that EAD thrust density is sufficient at the scale of unmanned aerial vehicles, where the available ratio of frontal area to weight is high, it is not currently sufficient for high-speed flight at the scale of commercial aviation: the area thrust density of our aeroplane was 3 N m^{-2}, that of a typical conventional unmanned aerial vehicle is of the order of 10 N m^{-2}, and that of a modern civil airliner is of the order of[7] 1,000 N m^{-2}.

Further improvements in these two performance limitations of overall efficiency and thrust density could enable EAD propulsion to open up new design spaces and unexplored applications for near-silent electric aircraft based on solid-state propulsion, in which the traditional limitations of propellers and gas turbines would no longer apply. Applications may include near-silent urban drones overcoming the current challenges of propeller noise, robust high-altitude environmental monitoring aeroplanes with no moving parts, and swarms of highly miniaturized solid-state-propulsion-based aircraft. The flight distances of 55 m and durations of 12 s for the heavier-than-air aircraft with solid-state propulsion described here compare well with the powered flight of the first heavier-than-air aircraft propelled by moving surfaces at Kitty Hawk, North Carolina, USA, 114 years ago. The Wright brothers achieved a flight[18] of 35 m lasting 11 s—although they did have to carry a pilot rather than a remote control unit.

Online content

Any methods, additional references, Nature Research reporting summaries, source data, statements of data availability and associated accession codes are available at https://doi.org/10.1038/s41586-018-0707-9.

Received: 22 June 2018; Accepted: 9 October 2018;
Published online 21 November 2018.

1. Chattock, A. P., Walker, W. E. & Dixon, E. H. IV. On the specific velocities of ions in the discharge from points. *Phil. Mag.* **1**, 79–98 (1901).
2. Stuetzer, O. M. Ion-drag pumps. *J. Appl. Phys.* **31**, 136–146 (1960).
3. Christenson, E. A. & Moller, P. S. Ion-neutral propulsion in atmospheric media. *AIAA J.* **5**, 1768–1773 (1967).
4. Wilson, J., Perkins, H. D. & Thompson, W. K. *An Investigation Of Ionic Wind Propulsion.* Report No. NASA/TM 2009–215822 (NASA, 2009).
5. Masuyama, K. & Barrett, S. R. H. On the performance of electrohydrodynamic propulsion. *Proc. R. Soc. A* **469**, 20120623 (2013).
6. Monrolin, N., Plouraboué, F. & Praud, O. Electrohydrodynamic thrust for in-atmosphere propulsion. *AIAA J.* **55**, 4296–4305 (2017).
7. Gilmore, C. K. & Barrett, S. R. H. Electrohydrodynamic thrust density using positive corona-induced ionic winds for in-atmosphere propulsion. *Proc. R. Soc. A* **471**, 20140912 (2015).
8. Loeb, L. B. *Electrical Coronas: Their Basic Physical Mechanisms* (Univ. California Press, Berkeley, 1965).
9. Melcher, J. R. Traveling-wave induced electroconvection. *Phys. Fluids* **9**, 1548 (1966).
10. Allen, P. H. G. & Karayiannis, T. G. Electrohydrodynamic enhancement of heat transfer and fluid flow. *Heat Recovery Syst.* **15**, 389–423 (1995).
11. Drew, D. S., Lambert, N. O., Schindler, C. B. & Pister, K. S. J. Toward controlled flight of the ionocraft: a flying microrobot using electrohydrodynamic thrust with onboard sensing and no moving parts. *IEEE Robotics Automation Lett.* **3**, 2807–2813 (2018).
12. Cumpsty, N. & Heyes, A. *Jet Propulsion* (Cambridge Univ. Press, Cambridge, 1998).
13. Leishman, J. G. *Principles of Helicopter Aerodynamics* (Cambridge Univ. Press, Cambridge, 2000).
14. Hoburg, W. & Abbeel, P. Geometric programming for aircraft design optimization. *AIAA J.* **52**, 2414–2426 (2014).
15. Gu, W. J. & Liu, R. A study of volume and weight vs. frequency for high-frequency transformers. In *Power Electronics Specialists Conf.* 1123–1129 (IEEE, 1993).
16. He, Y., Woolston, M. R. & Perreault, D. J. Design and implementation of a lightweight high-voltage power converter for electro-aerodynamic propulsion. In *IEEE Workshop on Control and Modeling for Power Electronics* http://doi.org/10.1109/COMPEL.2017.8013315 (IEEE, 2017).
17. Hsu, W. C., Chen, J. F., Hsieh, Y. P. & Wu, Y. M. Design and steady-state analysis of parallel resonant DC–DC converter for high-voltage power generator. *IEEE Trans. Power Electronics* **32**, 957–966 (2017).
18. McFarland, M. W. (ed.) *The Papers of Wilbur and Orville Wright* (McGraw-Hill, New York, 1953).

Acknowledgements The work was also contributed to by many undergraduate students from 2010–2018 as part of MIT's Undergraduate Research Opportunities Program (UROP), as part of MIT's Minority Students Research Program (MSRP), or as part of MIT's summer research exchange program with Imperial College London (IROP). These students include Y. K. Tey, P. Kandangwa, W. B. Rideout, J. Epps, S. O'Neill, M. Adams, J. M. Salinas, N. H. Rodman, I. L. LaJoie, W. A. Rutter, A. J. Sanders, N. J. Martorell, I. Vallina Garcia, J. P. Liguori, K. Dasadhikari, B. J. Scalzo Dees, M. H. Knowles, D. W. Fellows and D. P. Aaradhya. In addition, we thank A. Brown, T. Tao, C. Tan, P. Lozano, J. Peraire and C. Guerra-Garcia for technical discussions and advice, in some cases as part of student thesis committees. K. Masuyama, A. Dexter and J. Payton contributed to the project in its earlier phases. J. Leith and J. L. Freeman contributed to the financial and procurement administration for the project. F. Allroggen contributed to the resource management for the project. We also thank the laboratory staff at MIT AeroAstro for their help with the design, fabrication and flight testing of the EAD aircraft, in particular D. Robertson, T. Billings, A. Zolnik and T. Numan. Finally, we thank the MIT Department of Athletics, Physical Education, and Recreation for access to space for indoor flight testing, in particular S. Lett. This work was funded through MIT Lincoln Laboratory Autonomous Systems Line, the Professor Amar G. Bose Research Grant, and through the Singapore-MIT Alliance for Research and Technology (SMART). The work was also funded through the Charles Stark Draper and Leonardo career development chairs at MIT. This material is based on work supported by the Assistant Secretary of Defense for Research and Engineering under Air Force Contract No. FA8721-05-C-0002 and/or FA8702-15-D-0001. Any opinions, findings, conclusions or recommendations expressed in this material are those of the author(s) and do not necessarily reflect the views of the Assistant Secretary of Defense for Research and Engineering.

Reviewer information *Nature* thanks D. Drew, K. Pister, F. Plouraboué and H. Smith for their contribution to the peer review of this work.

Author contributions S.R.H.B. conceived the aeroplane. H.X. and C.K.G. designed the aeroplane. Y.H., D.J.P. and M.R.W. developed the electrical power systems. H.X., Y.H., K.L.S., C.K.G., S.P.K. and C.C.H. built and tested the aeroplane. H.X. piloted the aeroplane. K.L.S. and S.P.K. performed wind tunnel tests. S.R.H.B., D.J.P. and T.S. coordinated the project.

Competing interests The authors declare no competing interests.

Additional information
Extended data is available for this paper at https://doi.org/10.1038/s41586-018-0707-9.
Supplementary information is available for this paper at https://doi.org/10.1038/s41586-018-0707-9.
Reprints and permissions information is available at http://www.nature.com/reprints.
Correspondence and requests for materials should be addressed to S.R.H.B.
Publisher's note: Springer Nature remains neutral with regard to jurisdictional claims in published maps and institutional affiliations.

METHODS

Aircraft design optimization. The geometric programming optimization, used to produce a minimum-wingspan aircraft, was implemented using the open source Python library GPkit. Geometric programming is a convex optimization method able to efficiently find the global optimum for a certain objective function given a series of constraints[14]. Geometric programming constraints are formulated as monomial or posynomial inequalities, which under a log transformation, are convex functions. The constraints used in our model were composed of flight equilibrium constraints, and drag, weight, structural, propulsion system and electrical models. As an example, the flight equilibrium constraint requires lift to be equal to the weight of the aircraft multiplied by some load factor n, which is 1 for steady-level flight:

$$nW \leq \frac{1}{2}\rho v_0^2 S C_L$$

where W is the weight of the aircraft, v_0 is the aircraft speed, S is the wing planform area, and C_L is the vehicle lift coefficient.

Some constraints were implemented through the fit of surrogate geometric programming compatible functions to outputs from higher-fidelity models. For example, the wing profile drag and lift coefficients were calculated for a range of Reynolds numbers using the two-dimensional viscous panel program XFOIL. The XFOIL output was fitted to a geometric-programming-compatible posynomial function, and used as part of the optimization. A total of 93 constraints were used in the GPkit model to solve for a set of 90 free design variables.

Electrical systems. The electrical system consisted of a battery pack and an HVPC. The battery was composed of 54 3.7-V E-Flite 150 mAh Li-Po (lithium-ion polymer) cells connected in series. This cell was chosen for its high discharge rate (45 C), which allowed a peak discharge current of 6.75 A. The nominal operating voltage of the battery stack was 200 V, but could vary between 150 V and 225 V depending on the state of charge and discharge rate. The battery could sustain a 600 W discharge power for approximately 90 s. The duration of the flight tests was limited by the length of the indoor space, rather than by battery endurance.

The custom-designed HVPC used a conventional topology consisting of an inverter, a high-voltage transformer and a Cockcroft–Walton rectifier (Fig. 1c). The inverter converts the battery pack voltage to a 500–700 kHz alternating current with a voltage gain of approximately 2.5. The high-voltage transformer steps this up with a 1:15 voltage gain to an approximately 7-kV alternating current. The Cockcroft–Walton multiplier rectifies the 7-kV alternating current and multiplies it with a voltage gain of 5.6, producing a direct-current voltage of up to 40.3 kV. The efficiency of the HVPC was 82%–85% depending on the output power draw.

Laboratory and wind tunnel tests. The static performance of the thruster was evaluated by hanging the aeroplane vertically from a laboratory scale and measuring the change in measured force when the thruster was turned on. This was used to estimate the thrust of the aeroplane in flight.

The dynamic thrust performance of a section of thruster was measured in a 0.48 m by 0.48 m open jet wind tunnel at 0 m s^{-1}, 2 m s^{-1} and 5 m s^{-1} using a Pitot tube wake momentum survey. The testing confirmed that EAD thrust remained constant at 1 N m^{-1} span as velocity increased, in agreement with theoretical predictions for low speeds, but the net force decreased as velocity increased owing to an increase in parasitic drag on the electrodes.

Flight tests. We conducted flight tests in the Johnson Athletic Track at MIT. The indoor space was chosen so that the aircraft could be operated in a controlled environment, minimizing the effects of wind and temperature. The space had a useable length of 60 m.

During powered flights, the aeroplane was launched and maintained on a straight and steady flight path. The rudder and elevator surfaces were actuated with electronic servos: they were trimmed for straight flight, but adjusted during flight by the pilot via remote radio control, in particular during launch and landing. Around 5–10 m from the end of the flight area, the HVPC was remotely powered off, and the aircraft glided to ground (Supplementary Video 1). Extended Data Fig. 2 shows the HVPC output voltage and input power during a flight.

Not all flights resulted in the same height or energy gain. Variation was introduced by (1) piloting inconsistencies in the application of rudder and elevator control, which increased energy dissipated by aircraft drag, and (2) mechanical damage to the electrodes between flights. Crashed landings at the ends of flights 1, 2 and 5, which caused physical damage to the electrodes, and their subsequent field repairs, resulted in varying thrust performance.

During unpowered glides, the propulsion system was not turned on (Supplementary Video 2). The plane was trimmed appropriately for the unpowered condition, and after launch, the pilot attempted to maintain the aeroplane at a nominal angle of attack. The loss of height was due to drag alone and not improper trim or pitch control.

Aircraft video tracking. To demonstrate that the aircraft had achieved steady-level flight, we needed accurate measurements of both the height above the ground (for gravitational potential energy), and the velocity (for kinetic energy). We developed a motion capture system for tracking of the aircraft over the 60 m flight space using four GoPro Hero 5 Black cameras operating at 60 frames per second and a resolution of 2,704 × 1,520 pixels. Three of these cameras were directed perpendicular to the flight path to track the aircraft position in the x–z (fore–aft and up–down) plane. The fourth was directed in the direction of flight to track in the y (spanwise) direction.

Two LED lights, one green and one red, were placed on the pylon and the tail of the aircraft, respectively, to allow triangulation of the centre of gravity and calculation of the pitch angle. These lights were located on each image frame using MATLAB's Computer Vision toolbox. The computer vision tracking error was estimated by the average radius of these coloured regions, which was 0.05–0.07 m.

The raw output images from the cameras were subject to lens distortion, which was corrected using MATLAB's Image Processing and Computer Vision toolbox. A set reference images were produced using physical markers spaced 5 m by 3 m by 1 m in the x, y and z directions. There was a root-mean-square error of 0.045 m between a reference point position estimated by camera tracking, and the real-world position of the reference point.

The error in position tracking was estimated in two ways. The first was calculated as the sum of the computer vision tracking error, which was estimated from the size of the colored regions, and the lens correction error, which was estimated by the root-mean-square error of the reference point positions. The second was calculated from the regions of overlap between the cameras, where the plane was simultaneously in the field of view of more than one camera. By comparing the position reported by one camera with that simultaneously reported by another, a second estimate of each camera's tracking error was obtained. These errors were of similar magnitude, and the greater of the two errors was used to estimate the overall tracking error. This was 0.10–0.15 m depending on the particular flight, and this is the error shown in Figs. 3 and 4.

Data availability

The data that support the findings of this study are available from the corresponding author upon reasonable request.

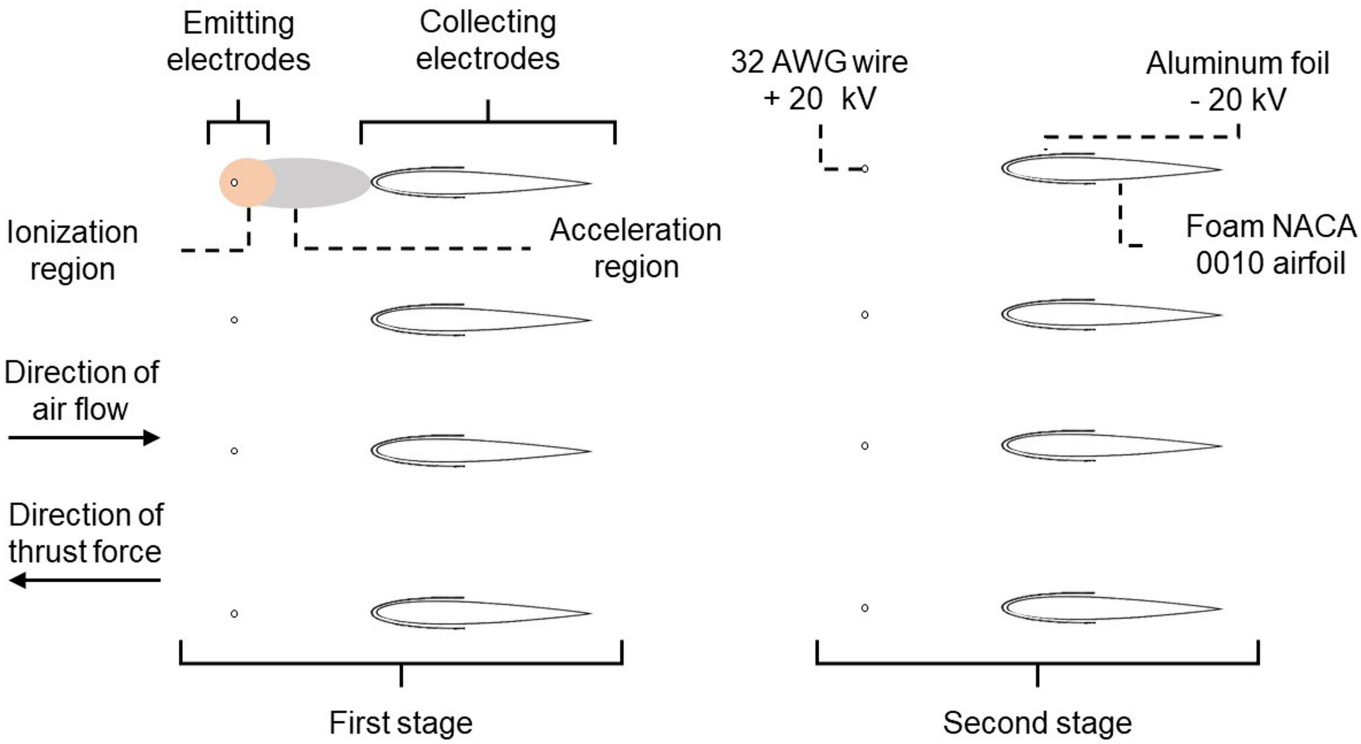

Extended Data Fig. 1 | Schematic of propulsion system electrodes. Not to scale. The emitting electrode is a 32 American Wire Gauge (32 AWG; 0.2 mm diameter) stainless steel wire, held at 60 mm spacing from the collecting electrode by 3D-printed spacers. The collecting electrode is a National Advisory Committee for Aeronautics (NACA) 0010 airfoiled foam section covered in a thin layer of aluminium foil. The electrodes are 3 m in span (into the page).

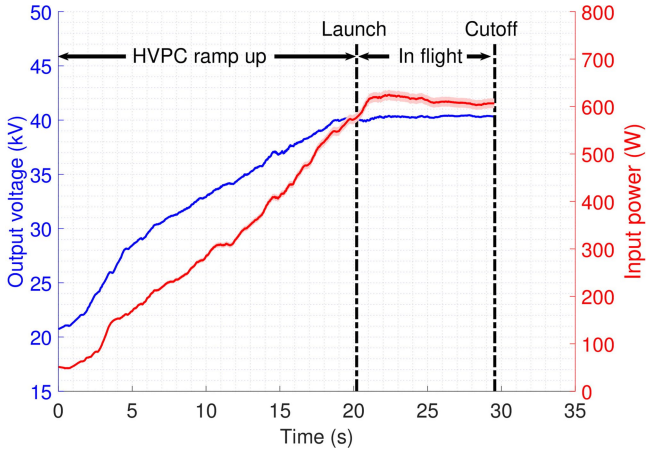

Extended Data Fig. 2 | HVPC output voltage and input power for a single flight (number 9). The HVPC is designed to ramp up to the final voltage over 20 s while the aeroplane is on the launcher. The aircraft was in flight for 10–12 s. During flight, the HVPC regulates the output voltage to maintain 40.3 kV.

Extended Data Table 1 | Key engineering parameters and performance metrics of the EAD aeroplane

Mass Budget	Total (kg)	2.45
	Power converter (kg)	0.51
	Battery (kg)	0.23
	Wing (kg)	0.63
	Electrodes (kg)	0.41
Aerodynamic Characteristics	Wing Span (m)	5.14
	Flight Velocity (m/s)	4.8 ± 0.2
	Aspect Ratio	17.9
	Drag (N)	3.0 ± 0.2
	Lift/Drag Ratio	8 ± 1
EAD Propulsion System	Thrust (N)	3.2 ± 0.2
	Voltage (kV)	40.3 ± 0.1
	Power Requirement (W)	620 ± 20
	Thrust Frontal Area (m^2)	0.9

Thrust and drag values are estimated from flight test data, and laboratory and wind tunnel experiments. Aerodynamic performance uncertainties arise from flight tracking error (see Methods). Uncertainties in electrical data are the 95% confidence interval from onboard HVPC measurements.